Instantaneous Baseline Imaging Using Passive Ultrasonic Guided Waves from Fiber Bragg Grating (FBG) Sensors

RAPHAEL CARPINE, QUENTIN BAUDIS, ANTOINE GALLET, CLEMENT FISHER, ARNAUD RECOQUILLAY and BASTIEN CHAPUIS

ABSTRACT

The detection and quantification of damage plays a crucial role in several industries. Assessing their severity enables to schedule maintenance appropriately, optimizing costs and reducing risks. Thanks to their long range and high sensitivity to defects, ultrasonic guided waves allow for the Structural Health Monitoring (SHM) of various structures using only a small number of sensors. However, the use of traditional piezoelectric transducers requires extensive wiring installation that weighs on the SHM system's costs and that may affect its reliability, and is limited to certain temperature and radiation ranges. To that extent, Fiber Bragg Grating (FBG) sensors offer an alternative instrumentation solution that withstands much higher temperatures and radiation levels, with a simplified installation thanks to the multiplexing of several sensors on the same optical fiber. They do not allow for actuation however, but passive guided waves techniques can be used to reconstruct active signals by exploiting the ambient excitation created by Environmental and Operational Conditions (EOCs). Furthermore, these EOCs and especially temperature have a significant impact on ultrasonic signals (independently of the instrumentation used, active or passive), which often exceeds that of the sought-after defects and thus limits the use of a baseline acquired from the structure in its pristine state. The instantaneous baseline technique addresses this issue by using damage free signals of the current state to create a statistical baseline, from which similar paths can be compared. In this study, passive ultrasonic signals acquired experimentally from FBG sensors are used for corrosion imaging through an instantaneous baseline technique. A thick steel plate, which is damaged locally using accelerated corrosion, is instrumented with multiplexed FBGs as well as piezoelectric sensors. Passive ultrasonic signals are acquired by both FBG and piezoelectric sensors using a compressed air jet as the excitation source, and active signals generated with the latter are also used for comparison. The instantaneous baseline method is applied to the signals and coupled with classical imaging techniques such as RAPID. Results obtained from the FBG passive and piezoelectric passive and active setups are then compared and discussed.

Raphael Carpine, Quentin Baudis, Antoine Gallet, Clement Fisher, Arnaud Recoquillay, Bastien Chapuis, Universite Paris-Saclay, CEA, List, F-91120, Palaiseau, France

INTRODUCTION

Environmental and Operational Conditions (EOC) play a crucial role in ultrasonic guided waves based Structural Health Monitoring (SHM), as their influence on signals can be similar or even greater than that of the damage. Conventional SHM methods relying on reference signals acquired when the monitored structure is in its pristine state are therefore particularly sensitive to EOCs, which poses robustness and reliability issues.

To address these issues, the instantaneous baseline techniques rely only on signals from the structure's current state for damage detection. Proposed originally by Anton et al. [1], they are based on the statistical comparison of signals from similar paths (same length, material, etc.), using features extracted from these signals such as mean power, correlation with other signals, projection on singular vectors, wavelet energy, center frequency, etc. [1–3]. Outliers are then detected and identified as damaged paths, and the method can be linked to imaging techniques such as the Reconstruction Algorithm for Probabilistic Inspection of Damage (RAPID) for defect localization [4].

Classical instrumentation setups for guided waves SHM rely on piezoelectric transducers, usually made from lead zirconate titanate (PZT), which can emit and receive ultrasonic waves. Recent advances in optical fiber sensing enabled the detection of these waves from Fiber Bragg Gratings (FBG), using a technique called edge filtering [5, 6]. However, actuation is not possible using FBGs, so the estimation of pitch-catch signals from a full FBG instrumentation needs to resort to passive methods.

Passive methods were first introduced in the geophysical field, as a mean to reconstruct surface waves' Green function between multiple receiving stations from ambient seismic noise [7]. They were since applied to ultrasonic guided waves for similar purposes, thus eliminating the need for actuation in the instrumentation setup and making use of the otherwise inconvenient ambient mechanical noise [6, 8–10].

In this study, an instantaneous baseline technique based on the signals' phase is implemented on experimental passive measurements from 7 multiplexed FBG sensors. A corrosion defect on a thick steel plate is detected and localized from these signals, as well as passive and active signals from 7 PZT transducers and the associated hybrid PZT – FBG signals, for comparison.

METHODS

Passive signals reconstruction

Passive methods rely on the presence of an ambient excitation applied to the monitored structure, emerging from EOCs (airflow for an aircraft fuselages, liquid flow for pipes and ship hulls, etc.). This excitation is modeled as a diffuse field, that is a Gaussian random process, stationary in time, with the following covariance [8]

$$\langle n(\boldsymbol{x},\, t)\, n(\boldsymbol{y},\, s)\rangle = F(s-t)\, K(\boldsymbol{x})\, \delta(\boldsymbol{y}-\boldsymbol{x}), \tag{1}$$

where δ is the Dirac delta function, F is the source field's power spectral density in time domain, and K characterizes its spatial support, which is assumed to be a closed surface. Under these assumptions, the cross-correlation between signals u_i and u_j measured on

the structure at points $\boldsymbol{x}_i$ and $\boldsymbol{x}_j$ respectively, estimated as

$$C_{ij}(\tau,\, T) = \frac{1}{T}\int_0^T u_i(t)u_j(\tau+t)\mathrm{d}t, \tag{2}$$

satisfies the following equation

$$\lim_{T\to+\infty}\frac{\partial C_{ij}}{\partial \tau}(\tau) \propto F * \left(H_{ij}(\cdot) - H_{ji}(-\cdot)\right)(\tau), \tag{3}$$

where H_{ij} and H_{ji} are the transfer functions between points x_i and x_j, and x_j and x_i respectively. This way, the cross-correlation estimator C_{ij} can be used to build an approximation of transfer function H_{ij}, and therefore of the active signal between points x_i and x_j after a convolution with the desired emission signal. This may require a whitening process however, in order to get rid of the convolution by F in Eq. (3).

Due to some differences between the modeled and the actual ambient excitation, several techniques must often be used in addition to cross-correlation computing. To account for the non-stationarity of the excitation, a normalization process will be used in this study, and to account for its non-flat spectrum, the inverse passive filter [11] will allow for some whitening as well as electronic noise filtering.

Instantaneous baseline

The instantaneous baseline technique proposed in this study is based entirely on the signals' phase, as the normalization of passive signals from sensors with various sensibilities and Signal to Noise Ratios (SNR) (these differ between PZTs and FBGs) is a complex topic, that will be addressed in future works.

In this regard, a first phase correction process is applied to the signals, to account for the sensors position error introduced during installation, which could induce unwanted phase shifts among groups of paths assumed to be of equal length. For any ultrasonic signal u_{ij} between sensors i and j, that may be recorded directly from active measurements or reconstructed from passive ones, a new corrected signal $\tilde{u}_{ij}$ is introduced as

$$\tilde{u}_{ij} = \mathcal{F}^{-1}\left[\mathcal{F}[u_{ij}]\cdot\exp\left(2\mathrm{i}\pi\frac{\Delta d_{ij}}{\lambda_{A_0}}\right)\right], \tag{4}$$

where $\mathcal{F}$ denotes the Fourier transform, Δd_{ij} is the difference between the measured $i-j$ path length and its expected value, and λ_{A_0} is the theoretical wavelength of the A_0 mode as a function of frequency, computed from numerical simulations.

The signal phase is then defined as

$$\phi_{ij} = \arg\left(\mathcal{H}[\tilde{u}_{ij}](t_{ij})\right), \tag{5}$$

where $\mathcal{H}$ denotes the Hilbert transform and t_{ij} is the theoretical time of flight of path $i-j$, obtained from the theoretical A_0 group velocity, also computed from numerical simulations. A damage indicator DI_{ij} is derived from ϕ_{ij}, as

$$\mathrm{DI}_{ij} = \underset{(k,\,l)\,\in\,\Omega_p}{\mathrm{median}}\,\phi_{kl} - \phi_{ij}, \tag{6}$$

where $(\Omega_k)_k$ are the sets of same length paths and Ω_p is the one that contains path $i-j$. The use of a median rather than a mean value is to account for the potentially limited number of same length paths, which requires robustness to outliers. The sign of Eq. (6) is chosen so as to maximize DI_{ij} when the A_0 mode is slowed by a thickness loss on path $i-j$ (which is the defect created in the experimental section of this study), however an absolute value may be used for a more generic indicator.

At last, a threshold $\mathrm{DI}_{\text{thres.}}$ needs to be set in order to distinguish damaged paths from healthy ones. In an applied case, this should be done from previous experience of similar structures with similar instrumentation, however as those are not available yet, results from the pre-damage test sample will be used for this study.

RAPID imaging

The instantaneous baseline technique is then combined with RAPID imaging, to allow for damage localization after its detection. It defines a defect distribution probability estimation P from a superposition of ray ellipses, expressed as [4]:

$$P(\boldsymbol{x}) = \sum_i \sum_j \frac{F_{ij}}{\beta - 1} \left[\beta - \frac{\|\boldsymbol{x} - \boldsymbol{x}_i\|_2 + \|\boldsymbol{x} - \boldsymbol{x}_j\|_2}{\|\boldsymbol{x}_j - \boldsymbol{x}_i\|_2} \right]^+, \tag{7}$$

where F_{ij} is the damage feature of path $i-j$, $\boldsymbol{x}_i$ and $\boldsymbol{x}_j$ are the positions of the i^{th} and j^{th} sensors respectively, and $\beta > 1$ is a scaling parameter.

Damage features F_{ij}, commonly based on the correlation between reference and current state signals, are computed here from damage indexes DI_{ij} defined in the instantaneous baseline section, as

$$F_{ij} = \begin{cases} \mathrm{DI}_{ij}^2 & \text{if } \mathrm{DI}_{ij} \geq \mathrm{DI}_{\text{thres.}} \\ 0 & \text{else.} \end{cases} \tag{8}$$

RESULTS AND DISCUSSION

Experimental setup and protocol

A $1 \times 1\,\mathrm{m}^2$, 10 mm thick S355 carbon steel plate was used for experimental validation. A total of 14 sensors were glued to the plate, 7 FBGs and 7 PZTs, evenly distributed on a 500 mm diameter circle, each FBG aligned with its radius, as shown in Figure 1. The choice of this circular pattern was based a study from Motamet et al. [2], which demonstrated that it allows for better probability of detection and localization of defects than other patterns on average. FBG sensors were engraved on two separate fibers, one containing FBGs A* to E*, the other one F* and G*. An accelerated corrosion process was performed using electrolysis on a 78 mm diameter area, resulting in a 2 mm thickness loss (20 % of the total thickness).

Both the actuation and sensing of PZT transducers was handled by the Geronimo system, developed at CEA List and Université Gustave Eiffel and now marketed by RcosPi, allowing for arbitrary waveform generation, amplification, pre-amplification and digitization in 8 separate synchronized channels. Sensing of the FBGs was ensured by another

system developed at CEA List [6], capable of ultrasonic measurements sampled at 2 MHz on 7 (multiplexed) synchronized optical channels. This system uses edge filtering with wavelength tracking as a measuring technique – for more details see [6]. Both systems were synchronized with an electrical trigger.

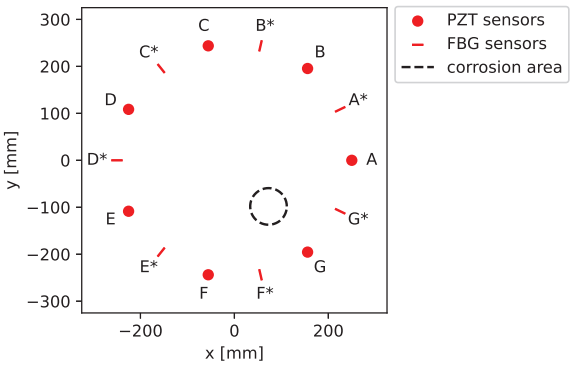

Figure 1. Experimental sensors layout.

Passive acquisitions were performed using a compressed air jet as the ambient excitation source, both systems recording simultaneously 50 s of signal sampled at 500 kHz. Some active acquisitions were also performed using the PZT transducers for actuation, with 3 cycles, Hann windowed pulses of amplitude 80 Vpp and center frequencies 20 kHz, 40 kHz and 60 kHz, sampled from both types of sensors at 2 MHz.

Passive signals reconstruction

The power spectral density of raw passive signals of a FBG sensor and of a PZT sensor are shown in Figures 2a and 2b respectively, with the air jet excitation (normal passive acquisition) and without (electronic noise only). Although it is whiter (flat spectrum with no peaks) and insensitive to electromagnetic interference along the (optical) cabling, the electronic noise in FBG channels is much higher than that of PZT sensors, and seems to meet the power of the mechanical noise around 50 kHz. As for the mechanical noise, it follows its typical exponentially decreasing shape after the high-pass filter of the systems, whose cut-off frequency lies around 10 kHz.

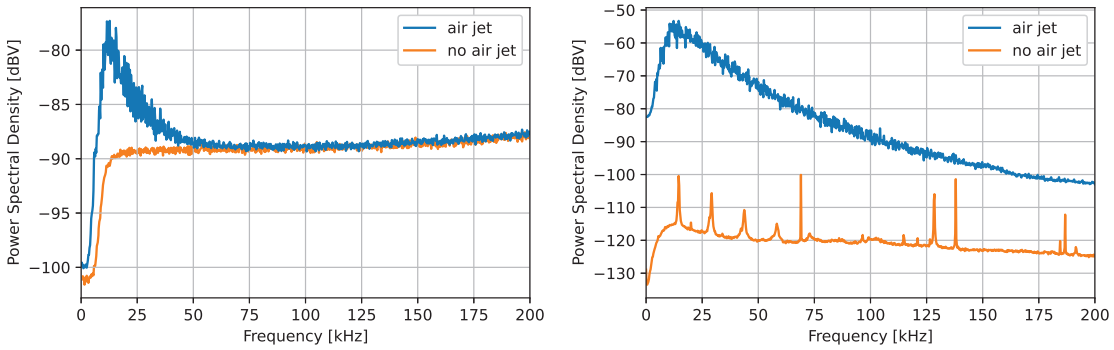

(a) FBG sensor

(b) PZT sensor

Figure 2. Examples of power spectra of raw passive signals from a PZT and a FBG sensor, with and without air jet excitation.

Examples of reconstructed passive signals, computed from the process described in the METHODS section followed by a convolution with 3 cycles pulses of various center frequencies, are plotted in Figure 3. Those from the FBG – FBG sensors pair show good reconstruction of the direct A_0 wave packet up until 50 to 60 kHz, and those from the PZT – FBG pair until 110 kHz at least, despite the negative SNR of the mechanical

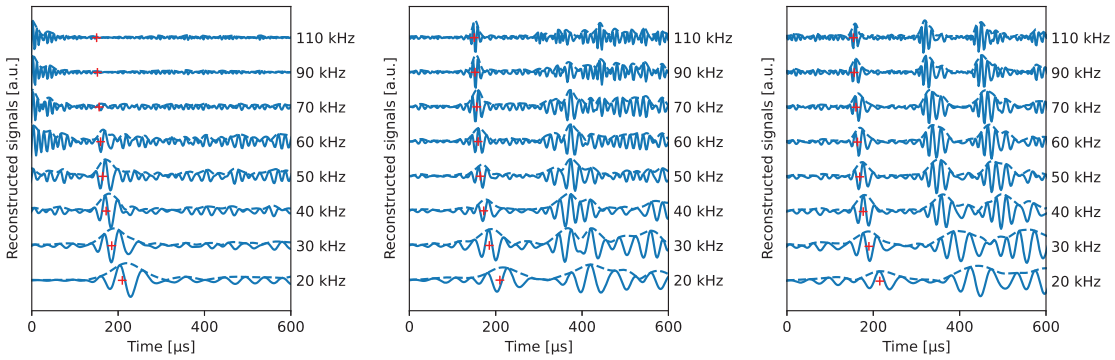

(a) FBG – FBG path (b) PZT – PZT path (c) PZT – FBG path

Figure 3. Examples of passive signals reconstruction on a FBG – FBG, a PZT – PZT and a PZT – FBG path, convoluted with 3 cycles pulses at various frequencies, with theoretical direct A_0 wave packet times of flight (red markers).

signals measured by FBGs at these frequencies as demonstrated by Figure 2a. This can be explained by the absence of correlation between the electronic noises of different acquisition channels, which are thus averaged out by the correlation computations, and allows for better signal reconstruction from FBGs than first expected.

Imaging results

The instantaneous baseline imaging technique described in section METHODS from Eqs. (4) though (8) is then applied on these reconstructed passive signals convoluted with 40 kHz pulses, as well as the 40 kHz active signals. CIVA Guided Waves software is used for the computation of the theoretical A_0 dispersion curves that are required for Eqs. (4) and (5). Only paths at least 391 mm apart are considered, as sensitivity of adjacent FBGs in their direct path is greatly reduced due to their directivity (angular sensitivity decrease in $\cos^2$). The number of paths in each of the equal length paths groups Ω_p is given in Table I for various sensor combinations.

TABLE I. Sizes of groups of equal length paths, for various sensor combinations.

Path length [mm]	500	487	450	391
FBG – FBG paths	–	7	–	7
PZT – PZT paths	–	7	–	7
PZT – FBG paths	7	–	14	–
All paths	7	14	14	14

Imaging results from passive and active (when relevant) measurements, considering only PZT – PZT paths, PZT – FBG paths, FBG – FBG paths or all of them, are presented in Figure 4. The corrosion defect is detected and localized in all cases, with a slight position error for same sensor type results (PZT – PZT and FBG – FBG) which originates from the low density of paths intersections of these setups. Passive results seem to compare with the corresponding active results, with the noticeable exception of a false positive path (B – D) in the PZT – PZT paths passive results (Figure 4b).

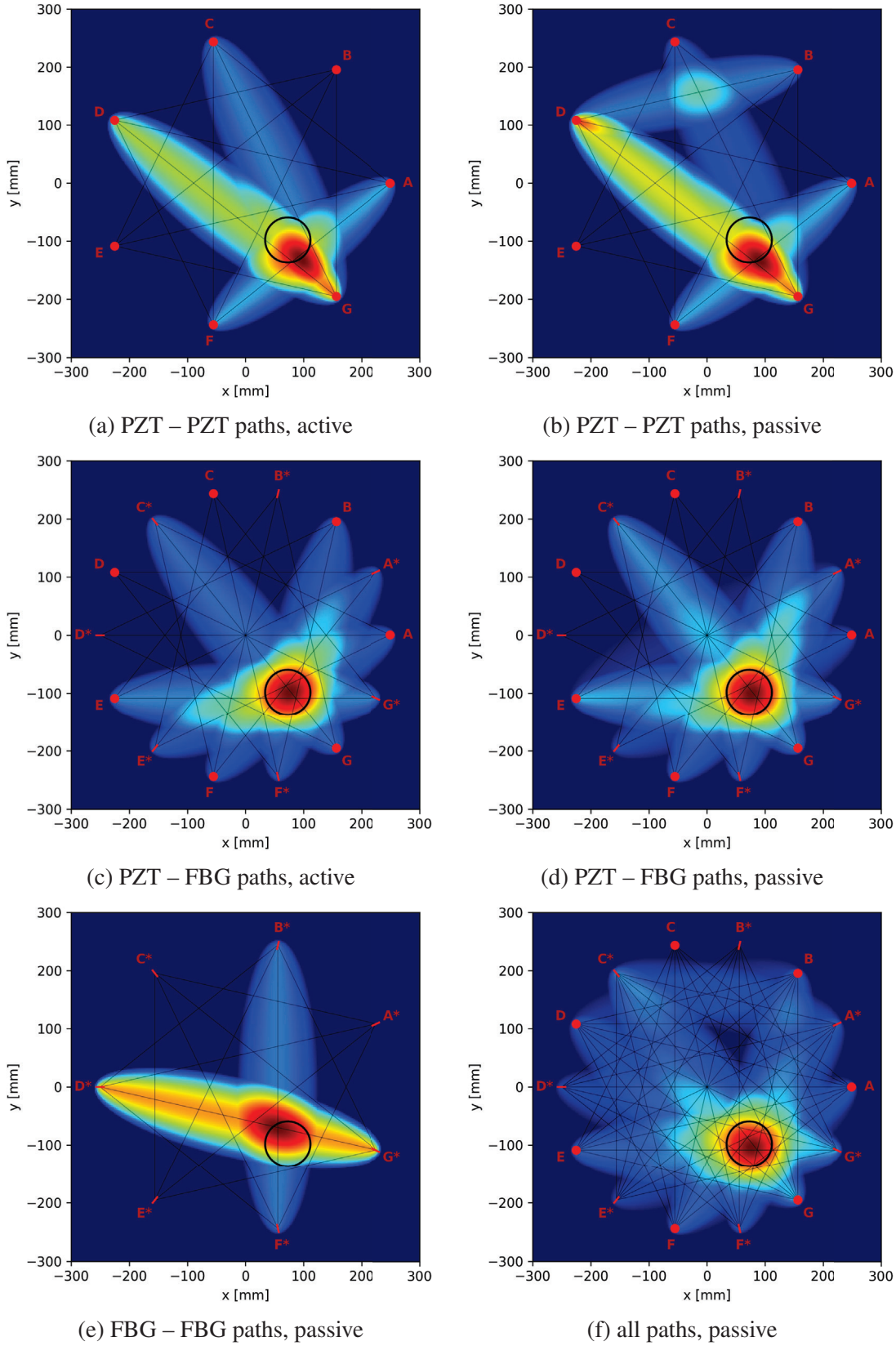

(a) PZT – PZT paths, active

(b) PZT – PZT paths, passive

(c) PZT – FBG paths, active

(d) PZT – FBG paths, passive

(e) FBG – FBG paths, passive

(f) all paths, passive

Figure 4. Instantaneous baseline combined with RAPID imaging results, from active and passive measurements, considering various sensor paths.

CONCLUSIONS AND PERSPECTIVES

In this study, an instantaneous baseline technique was implemented on experimental passive measurements from 7 multiplexed FBG sensors, as well as 7 PZT transducers. Results from both types of sensors allowed for the detection and localization of a corrosion defect on a 10 mm thick steel plate.

The perspectives of this study include the quantitative thickness mapping of similar structures from passive FBG measurements using guided waves tomography [9], and the normalization of passive signals from sensors with different sensibilities and SNRs.

ACKNOWLEDGMENT

This project has received partial funding from the European Defense Fund (EDF) under Grant agreement 101103257 – dTHOR – EDF-2021-NAVAL-R-2.

REFERENCES

1. Anton, S. R., G. Park, C. R. Farrar, and D. J. Inman. 2007. "On piezoelectric Lamb wave-based structural health monitoring using instantaneous baseline measurements," in T. Kundu, ed., *Health Monitoring of Structural and Biological Systems 2007*, SPIE, San Diego, California, vol. 6532, p. 65320B.
2. Motamed, P. K., A. Abedian, and M. Nasiri. 2020. "Optimal sensors layout design based on reference-free damage localization with lamb wave propagation," *Structural Control and Health Monitoring*, 27(4).
3. Mesnil, O., A. Recoquillay, C. Fisher, V. Serey, S. Sharma, and O. d'Almeida. 2023. "Self-referenced robust guided wave based defect detection: Application to woven composite parts of complex shape," *Mechanical Systems and Signal Processing*, 188:109948.
4. Hay, T. R., R. L. Royer, H. Gao, X. Zhao, and J. L. Rose. 2006. "A comparison of embedded sensor Lamb wave ultrasonic tomography approaches for material loss detection," *Smart Materials and Structures*, 15(4):946–951.
5. Jinachandran, S. and G. Rajan. 2021. "Fibre Bragg Grating Based Acoustic Emission Measurement System for Structural Health Monitoring Applications," *Materials*, 14(4):897.
6. Calmon, P., A. Recoquillay, N. Roussel, L. Maurin, T. Druet, G. Laffont, and B. Chapuis. 2023. "Towards Passive Fiber Bragg Grating-Based Measurement of Ambient Elastic Noise for SHM Under Varying Environment," in *Proceedings of the 14th International Workshop on Structural Health Monitoring*, Destech Publications, Inc., 978-1-60595-693-0.
7. Shapiro, N. M., M. Campillo, L. Stehly, and M. H. Ritzwoller. 2005. "High-Resolution Surface-Wave Tomography from Ambient Seismic Noise," *Science*, 307(5715):1615–1618.
8. Garnier, J. and G. Papanicolaou. 2016. *Passive Imaging with Ambient Noise*, Cambridge University Press, 1 edn., 978-1-107-13563-5 978-1-316-47180-7.
9. Druet, T., A. Recoquillay, B. Chapuis, and E. Moulin. 2019. "Passive guided wave tomography for structural health monitoring," *The Journal of the Acoustical Society of America*, 146(4):2395–2403.
10. Reed, N. and J. Corcoran. 2024. "Passive wall thickness monitoring using acoustic emission excitation," *NDT & E International*, 148:103241.
11. Gallot, T., S. Catheline, P. Roux, and M. Campillo. 2012. "A passive inverse filter for Green's function retrieval," *The Journal of the Acoustical Society of America*, 131(1):EL21–EL27.